European Journal of Medicinal Chemistry 46 (2011) 3887–3899

Contents lists available at ScienceDirect

European Journal of Medicinal Chemistry

journal homepage: http://www.elsevier.com/locate/ejmech

Original article

New insights into the structural requirements for pro-apoptotic agents based on 2,4-diaminoquinazoline, 2,4-diaminopyrido[2,3-*d*]pyrimidine and 2,4-diaminopyrimidine derivatives

María Font [a,*], Álvaro González [a], Juan Antonio Palop [b], Carmen Sanmartín [b]

[a] Sección de Modelización Molecular, Dpto de Química Orgánica y Farmacéutica, Facultad de Farmacia, Universidad de Navarra, Irunlarrea 1, E-31008 Pamplona, Spain
[b] Sección de Síntesis, Dpto de Química Orgánica y Farmacéutica, Facultad de Farmacia, Universidad de Navarra, Irunlarrea 1, E-31008, Pamplona, Spain

ARTICLE INFO

Article history:
Received 21 January 2011
Received in revised form
10 May 2011
Accepted 24 May 2011
Available online 31 May 2011

Keywords:
Cytotoxicity
Apoptosis
Structure–activity relationships
Quinazolin-2,4-diamine
Pyrido[2,3-*d*]pyrimidin-2,4-diamine
Pyrimidin-2,4-diamine

ABSTRACT

As a continuation of our work on new anti-tumoral derivatives with selective pro-apoptotic activity in cancer cells, we describe the synthesis and the preliminary evaluation of the cytotoxic and pro-apoptotic activities of a series of pyrimidin-2,4-diamine derivatives that are structurally related to quinazolin-2,4-diamine and pyrido[2,3-*d*]pyrimidin-2,4-diamine derivatives. We also describe the structure–activity relationship studies carried out on four series' of quinazolin-2,4-diamine, 2-(alkylsulfanyl)-*N*-alkyl- and 2-(alkylsulfanyl)-*N*-alkylarylpyrido[2,3-*d*]pyrimidine and pyrimidin-2,4-diamine derivatives.

The proposed preliminary pharmacophore consists of a flat heterocyclic ring, preferably a pyrido[2,3-*d*]pyrimidine, with two equivalent alkylarylamine chains, preferably *N*-benzyl- or *N*-ethylphenylamine, located in positions 2 and 4 of the ring, and with a preferred ALogP in the range 4.5–5.5. The nitrogen present in the central ring can act as hydrogen bond acceptors (HBA) whereas the amino group in the 4-position can act as a donor (HBD) or an HBA and the amino group in the 2-position can act as an HBD. On the basis of the analyzed structural profiles, different mechanisms of action can be suggested for the quinazolin-2,4-diamine, the 2-(alkylsulfanyl)-*N*-alkylpyrido[2,3-*d*]pyrimidin-4-amine and the pyrido[2,3-*d*]pyrimidin-2,4-diamine derivatives.

1. Introduction

The molecular players involved in the development of apoptosis, the cellular suicide mechanism that enables living organisms to control abnormal cell division, are becoming increasingly well-characterized and represent a set of new targets for the development of more effective and selective anti-tumor agents [1].

The development of new anti-tumor therapeutic tools has advanced greatly in the past decade; thus, approaches for the treatment of cancer have moved towards targeting the specific molecular alterations that occur in tumor cells, concentrating essentially on the development of both small molecules and biological agents that have shown remarkable clinical activity without the toxicity associated with conventional chemotherapy [2–4].

With this objective in mind, we have in recent years developed a broad research program aimed at obtaining new pro-apoptotic anti-tumor compounds that also show high selectivity over tumor cell lines, thus affecting to a lesser extent the non-malignant cells [5–11].

As previously reported [9,10], the design of the target compounds was carried out according to a molecular fragmentary approach [12–14] based on the available bibliographic information. This process involved the construction of a starting general structure (Fig. 1a), with a planar heterocyclic ring (quinazoline or pyrido[2,3-*d*]pyrimidine ring), selected as the central fragment that can act as a scaffold to carry two functionalized branches in positions 2 and 4, which are equivalent or different with the aim of evaluating the possible influence of the symmetry/asymmetry on the target activity [15]. The selected starting ring systems are involved in numerous biological activities – mainly concerning cancer – with action mechanisms related to folate metabolism inhibition, topoisomerase inhibition, the inhibition of diverse tyrosine kinases and apoptosis induction, amongst others [16–19]. As an example, of the eight small molecules currently marketed against oncology indications, three (Gefitinib, Fig. 1b; Erlotinib, Fig. 1c and Lapatinib, Fig. 1d) are from the 4-anilinoquinazoline class [20,21].

* Corresponding author. Tel.: +34 948 425 600X6509; fax: +34 948 425 648.
E-mail address: mfont@unav.es (M. Font).

0223-5234/$ – see front matter © 2011 Elsevier Masson SAS. All rights reserved.
doi:10.1016/j.ejmech.2011.05.060

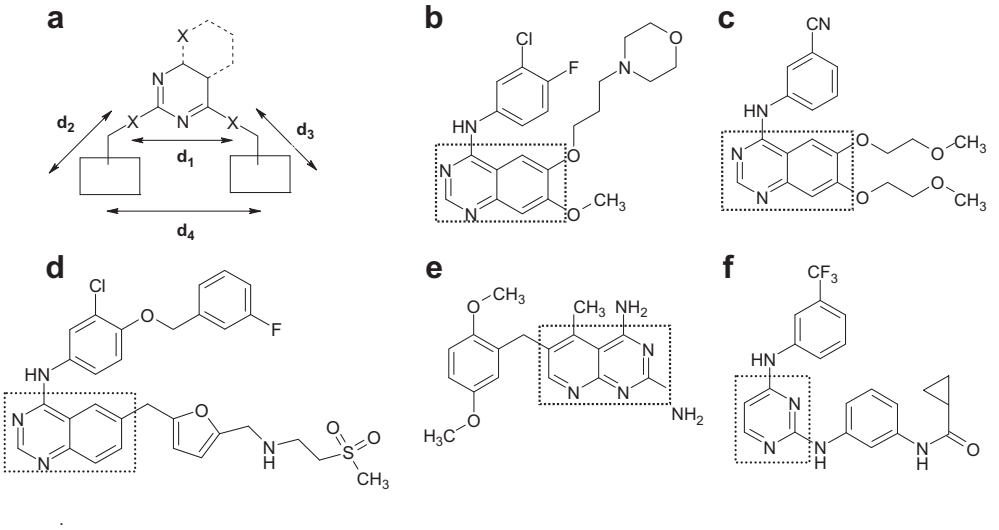

Fig. 1. (a) Preliminary pharmacophore (b) Gefitinib (c) Erlonitib. (d) Lapatinib. (e) Piritrexim (f) Aurora A kinase inhibitor. Structural modifications carried out on the central heteroaromatic nucleus taken as a scaffold (dotted lines): scaffold electronic modification, from quinazoline to pyrido[2,3-*d*]pyrimidine; scaffold simplification, from bicyclic to monocyclic system.

The importance of the lateral branches' length and volume, along with the presence of polar groups (like hydroxyl) at the end of the chain on the cytotoxic/pro-apoptotic activity were assessed [11,22]. We have also explored two different linkages to connect the side chains to the central ring. The first linkage was the amino group (−NH−), which was inserted in positions 2 and 4. Secondly, a sulfur atom was introduced in the 2-position [2-(alkylsulfanyl)-*N*-alkylpyrido[2,3-*d*]pyrimidin-4-amine derivatives] [11] maintaining an amino NH linkage at 4-position.

As a result of this approach we selected two new compounds, *N*,*N*′-dibenzyl aminoquinazolin-2,4-diamine (**3e**, Fig. 2) and *N*,*N*′-bis(4-methoxyphenyl)methyl pyrido[2,3-*d*]pyrimidin-2,4-diamine (**6ac**, Fig. 2), as leads for the subsequent design of other new compounds. Concerning the biological profile for these compounds, which showed good profiles as apoptosis inducers, we have demonstrated their activity as caspase-3 activators and inductors of DNA fragmentation in the micromolar (μM) range in several cancer cell lines. Tests were carried out to determine the possible mechanism of action for these selected compounds. The initial data highlighted how the observed dose-dependent cytostatic and pro-apoptotic effects resulted from the activation of two different signaling pathways, namely a pathway leading to cell cycle arrest and a transcription-independent route leading to rapid apoptosis [9,10].

In an effort to gain new insights into the structure−activity relationships for these compounds, we designed a series of new pyrimidine derivatives (compound **8**). This new derivatives, structurally related to the previously reported examples, implies a scaffold simplification associated with a significant diminution in the volume of the central nucleus as well as a change in the lipophilic profile. Three complementary new pyrido[2,3-*d*]pyrimidin-2,4-diamine (compounds **6v**, **6x**, **6y**) were also prepared. The proposed structural modifications on the scaffold were aimed at gaining some insight into the influence of parameters like the electronic distribution, lipophilicity and the total number of

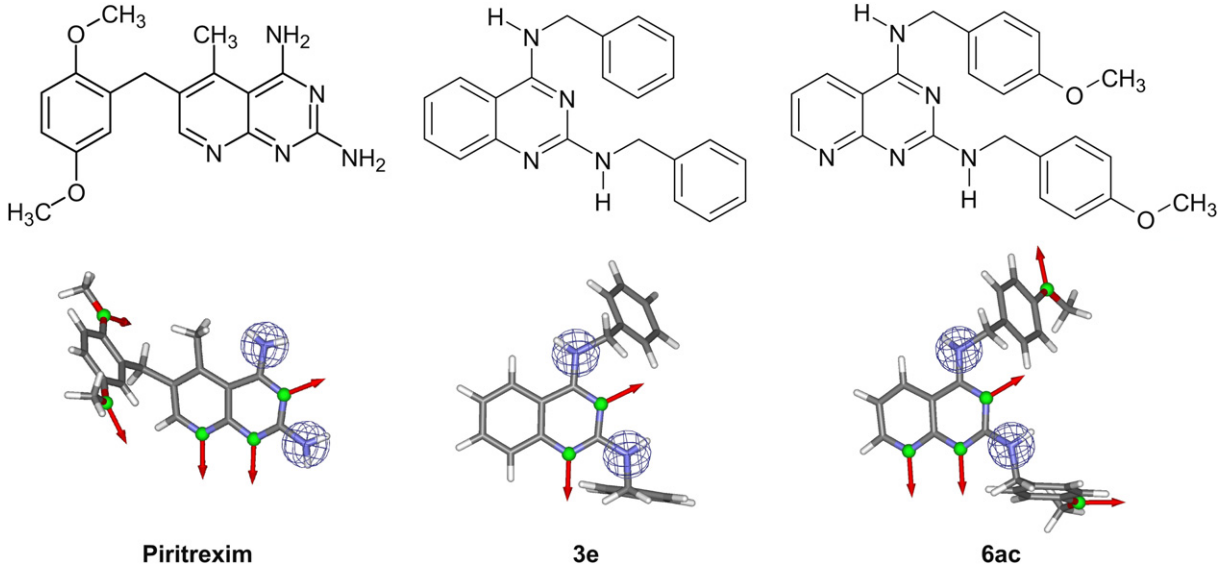

Fig. 2. H-bond donor (sphere) or acceptor (arrow) distribution pattern for compounds (a) Piritrexim, (b) **3e** (previously reported as JRF-12), (c) **6ac** (previously reported as HC-6).

nitrogens present in this central fragment [23], particularly in terms of the variation in the number of centers potentially involved in hydrogen bond formation.

We subsequently carried out a global molecular modeling study on the four series evaluated, i.e., quinazoline-2,4-diamine, pyrido[2,3-*d*]pyrimidin-2,4-diamine, 2-(alkylsulfanyl)-*N*-alkylpyrido[2,3-*d*]pyrimidin-4-amine and pyrimidin-2,4-diamine derivatives.

2. Results and discussion

2.1. Chemistry

The synthesis of the analyzed derivatives was carried out according to previously reported methods, which were adapted to the target structures (see Supplementary data for details). Thus, for the quinazoline derivatives **3** (synthesis not previously reported), 2,4-(1*H*,3*H*)-quinazolinedione was reacted in refluxing phosphorus oxychloride to afford 2,4-dichloroquinazoline. In a second step the chloro-substituents were replaced by the corresponding amines in the presence of ethanol as solvent (Scheme 1a).

The pyrido[2,3-*d*]pyrimidin-2,4-diamine derivatives **6** (Scheme 1b) were prepared from 2-aminonicotinic acid by condensation with excess urea to afford the pyrido[2,3-*d*]pyrimidin-2,4-diol. The hydroxyl groups were replaced by chloro-substituents by treatment with refluxing phosphorus oxychloride and *N*,*N*-dimethylformamide as catalyst. In the third step, the chloro-substituents were replaced by the corresponding amines in the presence of equimolecular amounts of triethylamine with ethanol as solvent.

Finally, the pyrimidin-2,4-diamine derivatives **8** were synthesized from the commercially available 2,4-dichloropyrimidine by treatment with an excess of the selected amines under reflux in ethanol (Scheme 1c).

The new synthesized compounds have been characterized unequivocally by means of IR, ^{1}H NMR and ^{13}C NMR spectroscopy techniques (see Supplementary data for details).

2.2. Biology

The method of evaluation of the new compounds was similar to that followed for the previously reported series of quinazoline and pyridopyrimidine derivatives [8–11]. The study of the biological profiles of the compounds involved the determination of the cytotoxic activity in three tumoral cell lines [breast (MD-MBA-231), bladder (T-24), and colon (HT-29)] using the neutral red assay at the screening concentrations of 100 and 20 μM, with camptothecin as the reference ($IC_{50} = 0.291$ μM in MD-MB-231 cell line, 0.014 μM in HT-29, and 0.006 μM in T-24). The survival percentage was determined after a period of 72 h using the survival percentage obtained from the cells treated only with the solvent (dimethylsulfoxide, DMSO at 0.5%) as a reference. The results are expressed as the average of assays carried out in triplicate. IC_{50} values were calculated for those compounds that showed survival levels of 45% (100 μM) in activity assays. The ability of the selected compounds to induce DNA fragmentation, which is considered a hallmark of apoptosis, was assessed using the Cell Death Detection ELISA Plus Kit (Roche) after 24 h of incubation with the compounds. The DNA degradation level measured in the control culture was taken as 1.

The compounds were also subjected to a caspase-3 activation assay. The enzyme level was measured at 14, 24 and 48 h using flow cytometry. The results are expressed by (+) when an increase of approximately 50% was detected and (++) when an increase of 100% or more was observed.

With regard to selectivity, cytotoxicity was determined in cell cultures of two non-tumoral lines (CRL-7899 and CRL-11233). The highest IC_{50} calculated in the three tumoral lines was selected as the test concentration for assays on non-tumoral cells.

The complete biological screening data, including the previously published data, are summarized in Table 1 in order to facilitate the understanding of the structure–activity analysis carried out on all four series of derivatives.

The data obtained for the evaluated new compound **6** confirmed our starting hypothesis, according to which the presence of a hydroxyl group at the end of the lateral branches (compounds **6x** and **6y**) leads to the disappearance of the cytotoxic activity. Similarly, the length of the lateral branches clearly has an influence on the results. Thus compound **6v** (with two hexylamine substituents in the 2- and 4-positions) is inactive.

With respect to compound **8**, all of the evaluated compounds showed cytotoxic activity apart from compound **8i**, which is inactive. Generally, the pyrimidine derivatives proved to be less active than the previously reported analogs derived from quinazoline and pyrido[2,3-*d*]pyrimidine [9,10]. In spite of this fact, five compounds (**8a**, **8c**, **8d**, **8e** and **8f**) proved to be cytotoxic and showed IC_{50} values below 10 μM in at least one cell line. In addition, **8a** showed values as an apoptosis inducer between 2.3 and 2.8 times higher than that of Camptothecin, which was used as the reference. In general, and in a similar way to the data collected for the previously studied series, it was observed that compounds had a more potent effect against the breast cancer cell line. Nevertheless, the active cytotoxic compound **8** did not show any selectivity in the tests carried out with the non-tumoral cell lines.

2.3. Molecular modeling

Three molecular modeling approaches were applied in the study described here. Firstly, it was envisaged that some descriptive parameter at a molecular level could be obtained – such as the log of the partition coefficient (ALogP 98 [24,25]), the dipole moment and the molecular volume – that would allow discrimination between active and inactive compounds. Secondly, we planned to study a number of quantum parameters, i.e., HOMO and LUMO orbitals, charge and molecular electrostatic potential (MEP) distribution. Thirdly, we planned to study the conformational behavior of the compounds in order to identify their preferred conformations and to perform a distribution analysis on the pharmacophoric elements. In fact, a given compound can be considered as a collection of multiple instances, one for each conformation. An active compound contains at least one active instance, characterized by a set of chemical functions with a certain spatial arrangement and molecular shape, while an inactive compound does not [7,26,27]. On the assumption that all of the active compounds bind to the same site, we would expect their binding conformations to have similar shapes.

In the molecular modeling studies we used the geometric data obtained for some structurally analogous molecules (Fig. 3) as a reference; these data were obtained from the Cambridge Structural Database [28] (CSD) and from the Brookhaven Protein Data Bank [29,30] (PDB).

The compounds FARRUM [31] (Gefitinib, Fig. 3a), GIBHUU [32] (Piritrexim, Fig. 3b), Trimetrexate (Fig. 3c) isolated from PDB refcode 1pd9 [33,34], and the ligand isolated from PDB refcode 2no3 [35] (Fig. 3d), among others, were taken as templates to build the quinazolin-2,4-diamine, pyrido[2,3-*d*]pyrimidin-2,4-diamine and pyrido-2,4-diamine derivatives. The bicyclic skeleton in the quinazoline or pyrido[2,3-*d*]pyrimidine derivatives and the pyrimidine ring in the pyrimidine derivatives were first superimposed onto the corresponding unit in the selected reference compounds. The lateral chains were constructed initially in an extended conformation, with the selected dihedrals (abcd and

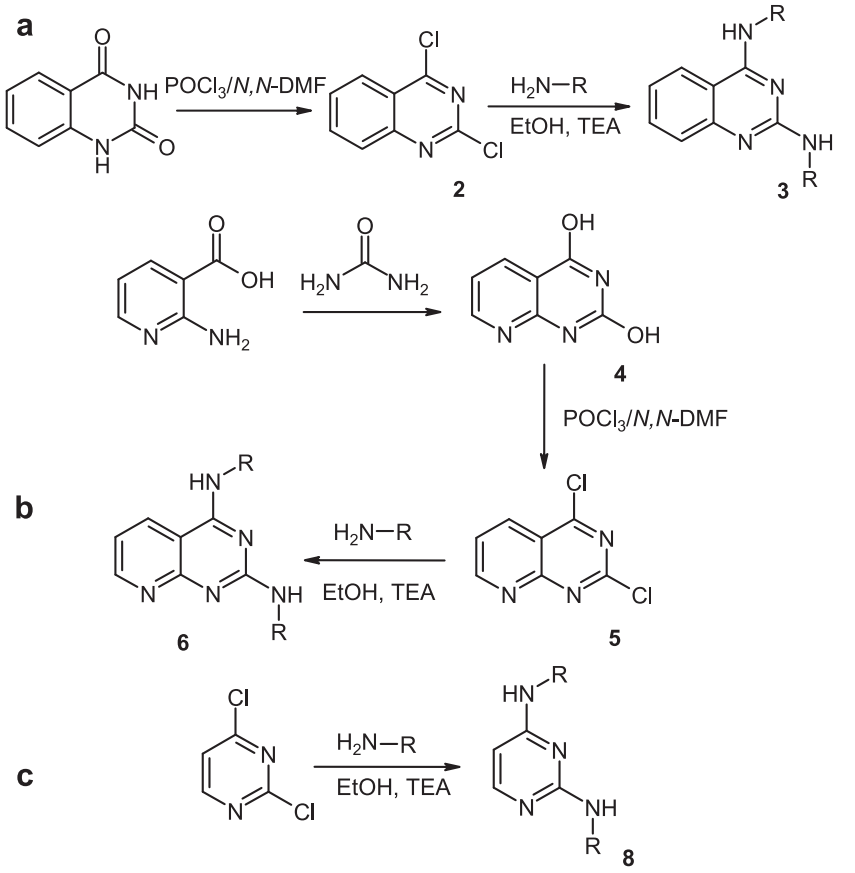

Comp.	R.	Comp.	R	Comp.	R
3a	-$(CH_2)_2CH_3$	**6t**	-$(CH_2)_3CH_3$	**8a**	-$CH_2C_6H_5$
3b	-$(CH_2)_3CH_3$	**6u**	-$(CH_2)_4CH_3$	**8b**	-CH_2-(4-CH_3-C_6H_4)
3c	-$(CH_2)_4CH_3$	**6v**	-$(CH_2)_5CH_3$	**8c**	-CH_2-(4-Cl-C_6H_4)
3d	-$(CH_2)_5CH_3$	**6w**	-$(CH_2)C_6H_5$	**8d**	-CH_2-(4-CH_3O-C_6H_4)
3e	-$(CH_2)_6CH_3$	**6x**	-$(CH_2)_3OH$	**8e**	-$(CH_2)_2C_6H_5$
3f	-CH_2-(4-CH_3-C_6H_4)	**6y**	-$(CH_2)_4OH$	**8f**	-$(CH_2)_3C_6H_5$
3g	-CH_2-(4-Cl-C_6H_4)	**6z**	-$CH_2C_6H_5$	**8g**	-$(CH_2)_4C_6H_5$
3h	-CH_2-(4-CH_3O-C_6H_4)	**6aa**	-CH_2-(4-CH_3-C_6H_4)		
3i	-$(CH_2)_2C_6H_5$	**6ab**	-CH_2-(4-Cl-C_6H_4)		
3j	-$(CH_2)_2$-(4-CH_3-C_6H_4)	**6ac**	-CH_2-(4-CH_3O-C_6H_4)		
3k	-$(CH_2)_2$-(4-Br-C_6H_4)	**6ad**	-$(CH_2)_2C_6H_5$		
3l	-$(CH_2)_3C_6H_5$	**6ae**	-$(CH_2)_2$-(4-Br-C_6H_4)		
3m	-$(CH_2)_4C_6H_5$	**6ah**	-$(CH_2)_3C_6H_5$		
		6ai	-$(CH_2)_4C_6H_5$		

Scheme 1. (a) Synthesis route for quinazoline derivatives **3**. (b) Synthesis route for pyrido[2,3-*d*]pyrimidine derivatives **6**. (c) Synthesis route for pyrimidine derivatives **8** (*N*,*N*-DMF = *N*,*N*-dimethylformamide; EtOH = Ethanol; TEA = *N*,*N*,*N*-triethylamine).

a'b'c'd', Fig. 3) in the *cis* configuration. The initial geometries were fully minimized with the Dreiding Minimize tool implemented in the Discovery Studio v2.5 suite (DS v2.5) to an energy gradient below 10^{-6} kcal mol^{-1} $Å^{-1}$ and the ALogP 98 value was determined on these preliminary geometries obtained after the first minimization (Table 2).

As predicted, the proposed structural variations caused a gradual modification in the lipophilicity of the compounds; thus, a wide range of ALogP 98 values was obtained, from 0.418 for **6x**, with hydroxyl groups present at the end of the side chains, to 7.700 for **3m**. In addition, an ample tolerance for these values was observed since some products with an ALogP 98 value higher than 7.0 showed remarkable cytotoxic activity, although generally the products with values below 3.0 were inactive in the cytotoxicity tests. This is the case for compounds like **3k** (ALogP 98 = 7.372 and IC_{50} = 3.32, 3.47 and 10.36 μM in T-24, HT-29 and MD-MBA-231 cell lines, respectively) or compound **6ai** (ALogP 98 = 7.462 and IC_{50} = 1.40, 5.00 and 1.10 μM in T-24, HT-29 and MD-MBA-231 cell lines, respectively).

The modification from quinazoline to pyrido[2,3-*d*]pyrimidine leads to a reduction in the ALogP values and this appears favorable

Table 1
Biological profile of compounds.

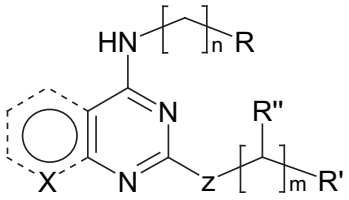

Comp.[a]	X	n	m	Z	R	R′	R″	IC_{50} (μM)[b]			Apoptosis in cell line[b]			Caspase-3[c]	Percent survival[b]	Percent survival[b]
								(a)	(b)	(c)	(a)	(b)	(c)		(d)	(e)
3a	C	2	2	NH	CH_3	CH_3	H	28.95	18.92	4.43	2.0	n.a.[d]	n.a.	n.a.	0	66
3b	C	3	3	NH	CH_3	CH_3	H	19.32	6.96	1.09	n.a.	1.5	n.a.	n.a.	4	1
3c	C	4	4	NH	CH_3	CH_3	H	5.25	3.57	3.13	1.8	1.7	2.5	+(T-24)	4	5
3d	C	5	5	NH	CH_3	CH_3	H	23.33	5.81	7.56	n.a.	n.a.	n.a.	–	2	0
3e	C	1	1	NH	C_6H_5	C_6H_5	H	5.96	4.72	1.79	n.a.	3.6	n.a.	++(T-24)	89	100
3f	C	1	1	NH	4-CH_3-C_6H_4	4-CH_3-C_6H_4	H	15.40	4.42	5.47	4.3	5.2	n.a.	n.a.	13	33
3g	C	1	1	NH	4-Cl-C_6H_4	4-Cl-C_6H4	H	6.41	5.89	4.26	2.0	n.a.	n.a.	n.a.	0	0
3h	C	1	1	NH	4-OCH_3-C_6H_4	4-OCH_3-C_6H_4	H	3.87	2.88	3.87	5.0	8.5	n.a.	+(HT-29)	0	100
3i	C	2	2	NH	C_6H_5	C_6H_5	H	2.86	2.30	2.18	n.a.	n.a.	n.a.	+(T-24)	92	100
3j	C	2	2	NH	4-CH_3-C_6H_4	4-CH_3-C_6H_4	H	2.17	1.64	4.65	n.a.	n.a.	2.4	+(HT-29)	0	0
3k	C	2	2	NH	4-Br-C_6H_4	4-Br-C_6H_4	H	3.32	3.47	10.36	n.a	n.a.	n.a.	+(T-24); +(HT-29)	11	1
3l	C	3	3	NH	C_6H_5	C_6H_5	H	3.45	2.20	4.18	n.a.	n.a.	n.a.	++(T-24); ++(HT-29)	87	2
3m	C	4	4	NH	C_6H_5	C_6H_5	H	11.90	3.78	1.22	n.a.	2.0	n.a.	++(T-24)	6	11
6a	N	1	1	S	CH_3	CH_3	H	20.10	26.20	18.70	1.3	n.a.	2.0	n.a.	–	–
6b	N	3	1	S	CH_3	CH_3	H	20.90	25.30	9.20	1.5	1.2	2.2	n.a.	–	–
6c	N	4	1	S	CH_3	CH_3	H	4.30	5.10	1.30	3.6	5.0	6.6	++(T-24); +(HT-29)	88	100
6d	N	5	1	S	CH_3	CH_3	H	5.90	22.50	1.40	1.5	8.1	3.3	++(HT-29); ++(MD-MBA-231)	n.d.[e]	n.d.
6e	N	6	1	S	CH_3	CH_3	H	5.30	19.90	2.60	n.a.	2.4	2.7	++ (T-24)	93	100
6f	N	3	1	S	OH	CH_3	H	n.a.	n.a.	n.a.	–	–	–	–	–	–
6g	N	4	1	S	OH	CH_3	H	n.a.	n.a.	n.a.	–	–	–	–	–	–
6h	N	5	1	S	OH	CH_3	H	n.a.	n.a.	n.a.	–	–	–	–	–	–
6i	N	3	1	S	CH_3	CH_3	CH_3	12.30	32.10	15.70	n.a.	n.a.	1.3	–	–	–
6j	N	4	1	S	CH_3	CH_3	CH_3	7.90	25.20	5.60	1.7	4.2	2.2	+(T-24); ++(HT-29)	100	66
6k	N	5	1	S	CH_3	CH_3	CH_3	15.80	20.20	4.50	1.6	n.d.[c]	2.9	n.a.	–	–
6l	N	6	1	S	CH_3	CH_3	CH_3	8.00	24.40	7.00	1.5	n.a.	n.d.	n.a.	–	–
6m	N	3	1	S	OH	CH_3	CH_3	n.a.	n.a.	n.a.	–	n.a.	n.a.	n.a.	–	–
6n	N	3	3	S	CH_3	CH_3	H	10.60	13.60	8.40	3.7	n.a.	n.d.	n.a.	–	–
6o	N	4	3	S	CH_3	CH_3	H	8.90	12.60	6.30	n.a.	1.9	1.7	+(T-24)	84	76
6p	N	5	3	S	CH_3	CH_3	H	4.50	2.80	1.20	4.3	6.4	9.3	++(T-24); ++(HT-29)	95	99
6q	N	3	4	S	CH_3	CH_3	H	n.a.	n.a.	n.a.	–	–	–	–	–	–
6r	N	4	4	S	CH_3	CH_3	H	n.a.	n.a.	n.a.	–	n.a.	–	–	–	–
6s	N	5	4	S	CH_3	CH_3	H	18.50	18.40	9.00	n.a.	n.a.	n.d.	n.a.	–	–
6u	N	4	4	NH	CH_3	CH_3	H	0.70	0.58	1.20	4.4	0.9	2.8	n.a.	100	54
6v	N	5	5	NH	CH_3	CH_3	H	4.60	4.23	2.10	–	–	–	–	–	–
6x	N	3	3	NH	OH	OH	H	n.a.	n.a.	n.a.	–	–	–	–	–	–
6y	N	4	4	NH	OH	OH	H	n.a.	n.a.	n.a.	–	–	–	–	–	–
6z	N	1	1	NH	C_6H_5	C_6H_5	H	13.40	11.00	10.30	4.6	2.5	n.a.	+(T-24)	85	90
6aa	N	1	1	NH	4-CH_3-C_6H_4	4-CH_3-C_6H_4	H	5.00	7.50	3.20	2.7	n.a.	4.0	n.d.	95	100
6ab	N	1	1	NH	4-Cl-C_6H_4	4-Cl-C_6H_4	H	11.00	15.00	8.30	1.9	n.a.	1.3	n.a.	0	100
6ac	N	1	1	NH	4-OCH_3-C_6H_4	4-OCH_3-C_6H_4	H	5.00	8.90	2.90	2.3	2.7	1.5	+(HT-29)	85	100
6ad	N	2	2	NH	C_6H_5	C_6H_5	H	8.10	2.50	1.20	1.2	9.2	n.a.	++(T-24); +(HT-29)	0	0
6ae	N	2	2	NH	4-Br-C_6H_4	4-Br-C_6H_4	H	11.50	4.10	2.70	1.5	7.2	n.a.	n.a.	90	100
6af	N	2	2	NH	2-pyridyl	2-pyridyl	H	n.a	n.a.	n.a	–	–	–	–	–	–
6ag	N	2	2	NH	3-indolyl	3-indolyl	H	7.70	3.00	5.10	n.a	3.0	n.a.	++(HT-29)	56	n.d.
6ah	N	3	3	NH	C_6H_5	C_6H_5	H	13.20	1.70	5.80	3.1	6	1.6	+(HT-29)	0	0
6ai	N	4	4	NH	C_6H_5	C_6H_5	H	1.40	5.00	1.10	4.6	1.4	n.a.	+(HT-29)	86	82
8a	–	1	1	NH	C_6H_5	C_6H_5	H	6.10	17.20	1.90	6	7.4	n.a.	n.a.	22	0
8b	–	1	1	NH	4-CH_3-C_6H_4	4-CH_3-C_6H_4	H	22.17	14.94	19.09	4.8	2.0	1.5	n.a.	6	1
8c	–	1	1	NH	4-Cl-C_6H_4	4-Cl-C_6H_4	H	8.50	9.80	2.0	n.a.	2.7	2.2	n.a.	0	n.d.
8d	–	1	1	NH	4-OCH_3-C_6H_4	4-OCH_3-C_6H_4	H	18.70	12.60	1.50	1.5	1.9	2.4	n.a.	0	n.d.
8e	–	2	2	NH	C_6H_5	C_6H_5	H	9.14	6.97	3.01	1.2	n.a.	1.3	n.a.	5	5
8f	–	3	3	NH	C_6H_5	C_6H_5	H	8.67	12.39	0.36	1.7	n.a.	3.2	+(HT-29)	10	1
8g	–	4	4	NH	C_6H_5	C_6H_5	H	n.a.	n.a.	n.a.	–	–	–	–	–	–

[a] Previously reported [9,10] as **3a** = JRF3; **3b** = JRF4; **3c** = JRF5; **3d** = JRF6; **3e** = JRF12; **3f** = JRF13; **3g** = JRF14; **3h** = JRF15; **3i** = JRF7; **3j** = JRF11; **3k** = JRF10; **3l** = JRF8; **3m** = JRF9; **6u** = VD14; **6v** = VD22; **6z** = HC1; **6aa** = HC2; **6ab** = HC3; **6ac** = HC6; **6ad** = XS1; **6ae** = XS4; **6af** = ME43; **6ag** = ME44; **6ah** = XS2; and **6ai** = XS3.
[b] Cell lines (a) T-24; (b) HT-29; (c) MD-MBA-231; (d) CRL-8799; and (e) CRL-11233.
[c] (+) an increase of 50% of caspase-3 level with respect to the control; and (++) an increase of 75% of caspase-3 level with respect to the control.
[d] n.a. = No activity observed after 48 h incubation.
[e] n.d. = No data.

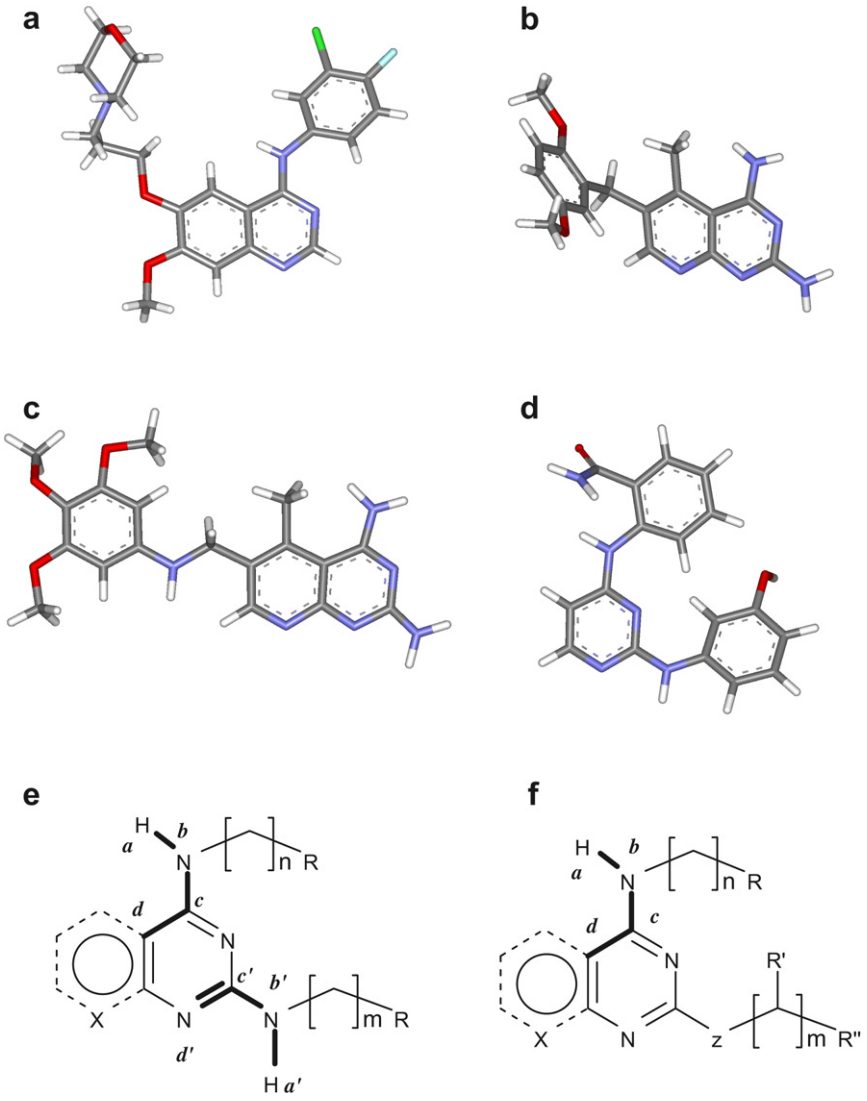

Fig. 3. Some crystallographic structures taken as geometric references (a) Gefitinib, CSD Refcode = FARRUM. (b) Piritrexim, CSD Refcode = GIBHUU. (c) Trimetrexate, ligand isolated from Brookhaven Protein Data Bank (PDB) Refcode = 1pd9. (d) Ligand isolated from PDB Refcode = 2no3. (e) and (f) Selected dihedrals (in solid) taken as a pattern value for conformational family distribution (A, abcd = a'b'c'd' ≈ 0°; B, abcd ≈ 0°, a'b'c'd' ≈ 180°; C, abcd ≈ 180°, a'b'c'd' ≈ 180°; D, abcd = 0°, a'b'c'd' = 180°).

for the target activity. For example, comparison of the activities for pairs of homologous compounds, e.g., **3c** and **6u** or **3d** and **6v**, with ALogP = 5.636 and 4.942 for **3c** and **6u**, respectively, and 6.548 and 5.854 for **3d** and **6v**, shows that compound **6**, with smaller ALogP value, has superior activity in the cytotoxicity and apoptosis tests carried out on the three cell lines. Similar observations were made for the pairs **3f**/**6aa** and **3h**/**6ac**.

Modification of the scaffold from pyrido[2,3-*d*]pyrimidine to pyrimidine also leads to a reduction in the value of ALogP 98. Comparison of the activity of homologous compounds **6** and **8** shows that the pyridopyrimidine derivatives have higher cytotoxic and pro-apoptotic activities.

The high ALogP values found for some active compounds contravene Lipinski's Rule of Five [36], which indicates the "drug-likeness" and according to which orally active drugs should have: (a) a molecular weight under 500 Daltons, (b) limited lipophilicity (expressed by Log $P < 5$, with $P = [\text{drug}]_{\text{org.}}/[\text{drug}]_{\text{aq.}}$), (c) a maximum number of 5 HBD (expressed as the sum of OH and NH groups) and (d) a maximum number of 10 HBA (expressed as the sum of Os and Ns).

The corresponding conformational analysis was carried out, having selected the rotatable bonds, by applying the Diverse Conformation Generation protocol implemented in the DS 2.5v suite. A set of 25–30 representative low energy conformations for each analyzed compound was selected (the energy differences between the different conformations analyzed for each trajectory were in the range 2–5 kcal; data not shown for the sake of brevity). The low energy conformers were superimposed onto the central nucleus of quinazoline, pyrido[2,3-*d*]pyrimidine or pyrimidine, as appropriate, with the N1, N2 and C2 of the pyrimidine ring taken as tethers. The effectiveness of the superimposed models was evaluated in terms of the root mean square (rms) values obtained.

The molecular volume was then calculated from the conformational trajectories and the mean values obtained for each analyzed compound were recorded (see Supplementary data). A wide range was observed for the mean molecular volumes. For the selected quinazoline derivatives that show the target activity, the average volumes are between 1000 and 1250 Å^3. In the case of the selected pyrido[2,3-*d*]pyrimidine derivatives, the average volumes are generally lower (869 Å^3 for compound **6c** and 1172 Å^3 for

Table 2
Molecular descriptors.[a]

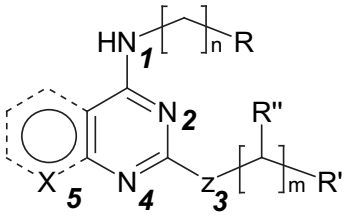

Comp.	AlogP 98	Dipole[b]	MEP[c]	HOMO[d]	LUMO[d]	$\Delta E_L - E_H$[d]
3a	3.811	3.411	1042.9	−8.309	−0.302	8.007
3b	4.723	3.319	896.5	−8.308	−0.296	8.012
3c	5.636	3.243	888.0	−8.299	−0.288	8.011
3d	6.548	3.420	600.7	−8.296	−0.295	8.001
3e	5.233	2.966	828.9	−8.441	−0.467	7.974
3f	6.205	3.934	1032.8	−8.353	−0.373	7.980
3g	6.562	2.155	859.3	−8.505	−0.693	7.812
3h	5.200	3.942	1002.9	−8.377	−0.414	7.963
3i	5.875	2.817	914.2	−8.401	−0.384	8.017
3j	6.848	3.401	614.9	−8.338	−0.324	8.014
3k	7.372	2.500	873.7	−8.513	−0.695	7.818
3l	6.788	2.999	645.9	−8.338	−0.329	8.010
3m	7.700	3.060	755.2	−8.365	−0.344	8.021
6a	2.803	5.146	606.7	−8.762	−1.055	7.707
6b	3.783	5.311	636.4	−8.748	−1.038	7.710
6c	4.239	5.160	564.9	−8.747	−1.035	7.712
6d	4.695	5.151	727.7	−8.749	−1.039	7.710
6e	5.151	5.144	641.8	−8.753	−1.044	7.709
6f	1.977	5.057	848.6	−8.793	−1.088	7.705
6g	2.557	5.129	769.1	−8.780	−1.382	7.398
6h	3.013	5.427	692.9	−8.772	−1.070	7.702
6i	4.160	5.179	631.9	−8.760	−1.052	7.708
6j	4.616	5.074	592.1	−8.751	−1.033	7.718
6k	5.073	5.274	496.8	−8.747	−1.032	7.715
6l	5.529	5.199	509.4	−8.749	−1.028	7.721
6m	2.354	4.846	800.4	−8.800	−1.085	7.715
6n	4.763	5.193	521.8	−8.736	−1.041	7.695
6o	5.219	5.290	538.3	−8.740	−1.042	7.698
6p	5.670	5.239	553.6	−8.744	−1.043	7.701
6q	5.219	5.332	639.6	−8.740	−1.049	7.691
6s	6.131	5.055	561.6	−8.750	−1.045	7.705
6u	4.942	5.625	992.7	−8.626	−0.532	8.094
6v	5.854	5.460	875.5	−8.653	−0.552	8.101
6x	0.418	5.003	1336.5	−8.877	−0.760	8.117
6y	1.578	4.063	1354.6	−8.698	−0.899	7.799
6z	4.539	5.091	977.4	−8.773	−0.699	8.074
6aa	5.511	5.826	1085.0	−8.775	−0.701	8.074
6ab	5.868	3.832	975.3	−8.699	−0.901	7.798
6ac	4.506	5.692	1219.4	−8.637	−0.596	8.041
6ad	5.181	5.382	984.9	−8.724	−0.623	8.101
6ae	6.678	3.749	1031.7	−8.700	−0.900	7.800
6af	3.164	6.549	1121.1	−8.692	−0.590	8.102
6ag	5.768	6.167	1318.8	−8.301	−0.545	7.756
6ah	6.094	5.096	911.6	−8.673	−0.579	8.094
6ai	7.462	5.390	826.4	−8.687	−0.589	8.098
8a	3.896	2.589	1106.0	−8.827	−0.045	8.782
8b	4.868	3.424	1153.8	−8.724	0.090	8.814
8c	5.225	1.678	1114.4	−8.805	−0.287	8.518
8d	3.863	3.920	1289.8	−8.675	0.054	8.729
8e	4.538	2.510	1077.9	−8.782	0.146	8.928
8f	5.451	2.448	806.3	−8.720	0.235	8.955

[a] Mean values obtained from conformational trajectory.
[b] Debyes.
[c] kT/e units (1 kT/e = 25.6 mV eV).
[d] In eV calculated on the lowest energy representative conformation.

compound **6ac**, taken as extreme values for derivatives that show the target activity and selectivity), although in this case, as for the active pyrimidine derivatives, the tolerance range is also wide.

The conformations obtained for each compound were distributed in families, taking as group criteria the overall value of the dihedrals abcd and a'b'c'd' (Fig. 3), which were selected as patterns for the analysis. The overall values for the dihedral angles allowed us to distinguish four conformational families: A, abcd = a'b'c'd' ≈ 0°; B, abcd ≈ 0°, a'b'c'd' ≈ 180°; C, abcd ≈ 0°, a'b'c'd' ≈ 180°; and D, abcd ≈ 180°, a'b'c'd' ≈ 0°. With respect to the 1,4-diamino derivatives, the preferred conformation for the majority of compounds is type A and this is followed by type B. Despite this conformational distribution, the lowest energy conformation for the most active compounds surprisingly corresponds to the type B family (see Supplementary data for details). As a representative example, the images obtained in the conformational study carried out on compounds **3e** and **6ac** are shown in Fig. 4. The H located on the N that acts as a linker for the lateral branch in position 4 is projected towards the pyridine ring in a similar way to the situation observed for the reference compounds (Fig. 3), whereas the H on the N acting as a linker for the branch in position 2 is projected towards N3 of the pyrimidine ring.

The preferred conformation in the 2-(alkylsulfanyl)-*N*-alkyl-pyrido[2,3-*d*]pyrimidin-4-amine derivatives is type A in all cases, with a value for the abcd dihedral close to 0º. The conformational variability of the pyrimidin-1,4-diamino derivatives is notable, since practically all of the studied compounds display a significant number of conformations assigned to the four families A, B, C and D.

In general, the lateral alkyl or alkylarylamino chains adopt an extended conformation, thus exploiting the molecular planarity. Exceptions include compounds like **6r** and **8g**, as illustrative examples, in which the lateral branches preferentially adopt a folded conformation (see Fig. 4). As a general pattern for the more active compounds, the aromatic rings located at the end of the side chain are projected differently with respect to the central ring plane; while the ring on the chain in position 2 preferentially forms an angle of ±90º with this plane, the ring in position 4 is located in a plane that forms an angle of ±30º (see Fig. 4). When the chain is sufficiently long ($n > 3$) the presence of OH groups causes the chain to fold, which in turn allows the formation of intramolecular H-bonds that involve the pyrimidine ring nitrogens and the sulfur atom in the 2-position, as well as the possibility of forming H-bonds that affect the OH group (Fig. 5). This framework of intramolecular H-bonds can stabilize the folded forms and can also lead to an increase in the value of ALogP.

The dipole moment (μ) was calculated and this was taken as an expression, from the asymmetry, of the overall molecular charge distribution and a quantitative measurement of the molecular polarity. The mean value (expressed in Debye units) for each trajectory is given in Table 2. Generally, derivatives **3** have lower μ values than derivatives **6**. On analyzing all of the dipole moment values it is possible to emphasize the greater asymmetry in the charge distribution for derivatives **6**, a situation that is not unexpected considering the modification of the central nucleus from quinazoline to pyrido[2,3-*d*]pyrimidine.

The molecular electrostatic potential (MEP) values for the analyzed compounds were calculated for the selected lowest energy conformations using the DS 2.5v Electrostatic Potential Protocol (EPP). The molecular electrostatic potential (MEP, in kT/e units) values were considered for the comparative analysis (see Supplementary data for details). The distribution of MEP values, taken as the potential energy of a proton at a particular location near a molecule, was calculated in order to evaluate the molecular zones that are able to participate as hydrogen bond donors or acceptors, with particular attention paid to the nitrogen and sulfur atoms present in the nuclear scaffolds and in the lateral branch linkages. Thus, a negative EP corresponds to an attraction of the proton by the concentrated electron density, whereas a positive EP corresponds to repulsion of the proton by the atomic nuclei in regions where low electron density exists and the nuclear charge is not completely shielded. As a general pattern (see Fig. 6 as an illustrative example), and with respect to the quinazolin-2,4-

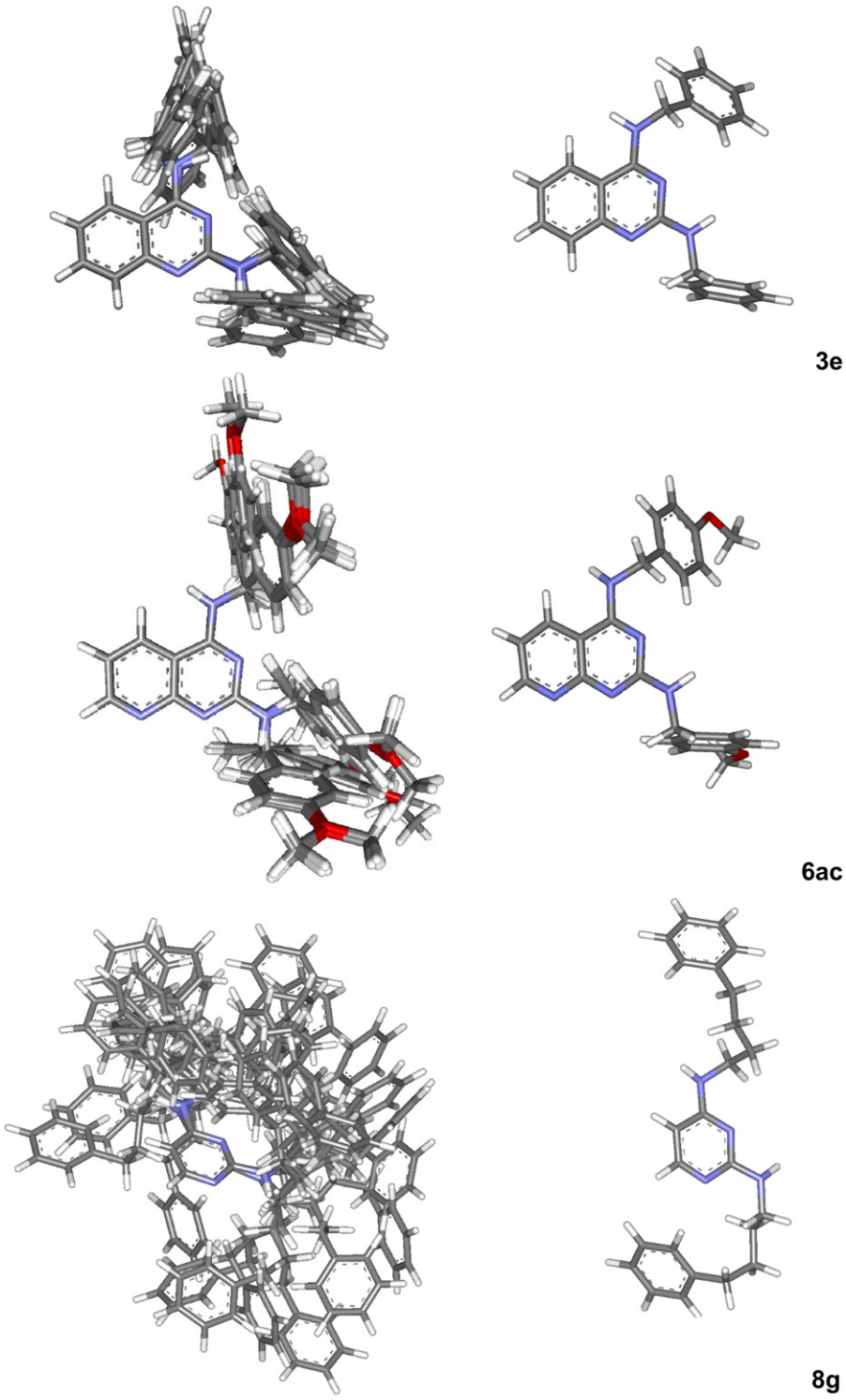

Fig. 4. Overlay of low energy conformations (left), taking the nitrogen atoms as tethers, and representative lowest energy conformation (right) for active compounds **3e** and **6ac**, and inactive compound **8g**.

diamine derivatives **3**, the negative EP values are preferentially located on the N atoms of the pyrimidine ring (N2 and N4) with a smaller contribution of nitrogens in positions 2 and 4 (N1 and N3).

The MEP values for compounds **6a**–**s** are lower than those obtained for compound **3** and the value for N1 is slightly positive, whereas that for S is slightly negative. The presence of N5 contributes an additional negative center and this is able to act as an HBA.

For compounds **6aa**–**ai** and for compound **8**, the MEP values are quite similar to those obtained for compound **3** with regard to nitrogens in the pyrimidine ring. However, the presence of N5 gives rise to a zone with very negative average values and nitrogen N1 is more negative than that in compound **3**. As a general pattern, the negative EP values are preferentially located on N atoms in the central scaffold (N2, N4 and N5 for compound **6**, and N2 and N4 for

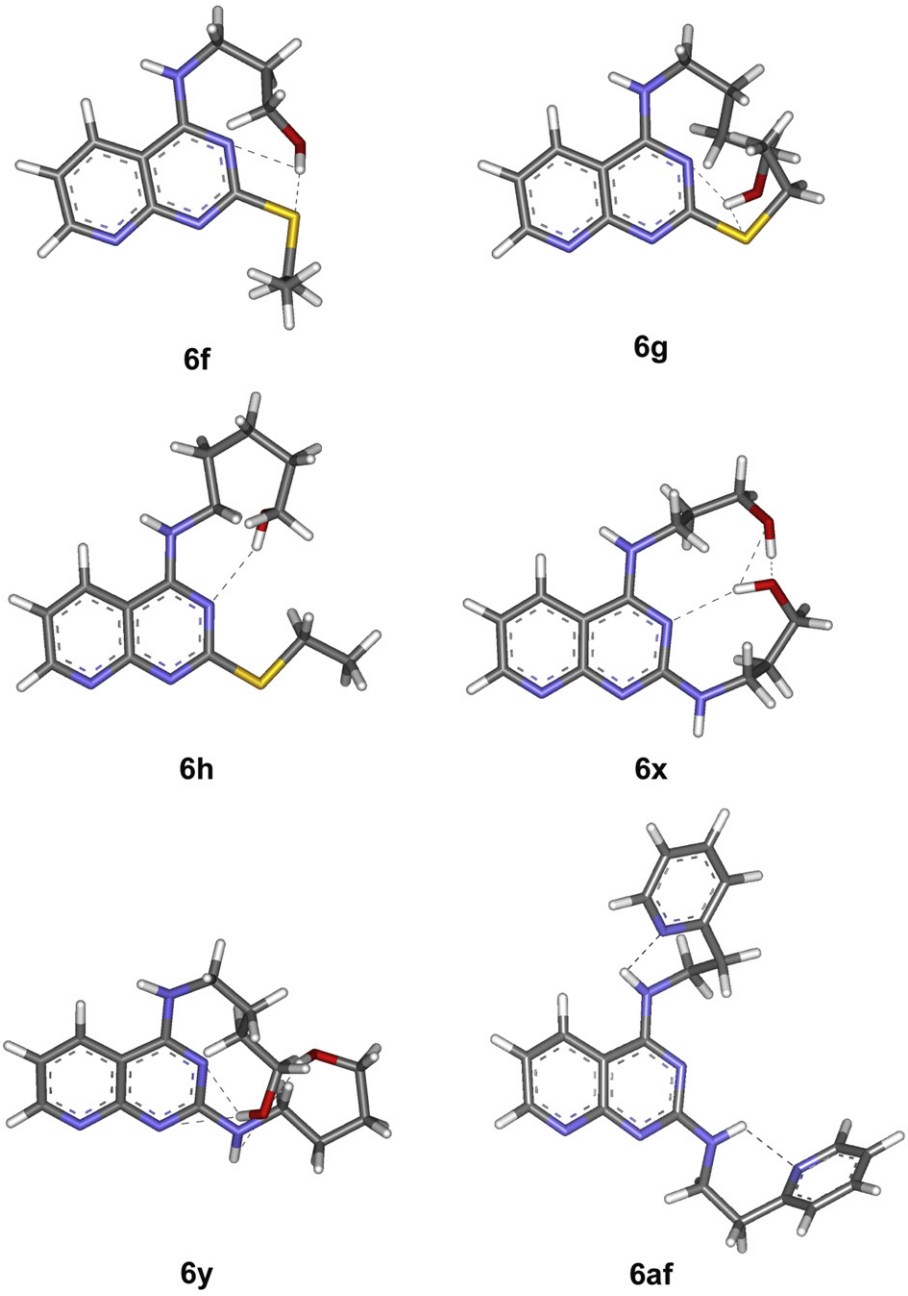

Fig. 5. Intramolecular H-bond (dotted line) pattern for some representative compounds.

compound **8**), with a smaller contribution from nitrogens in positions 2 and 4 (N1 and N3).

Finally, as quantum parameters (Table 2) the energy and distribution of HOMO 0 and LUMO 0 orbitals, the difference between the molecular orbital energies (gap), and the net atomic charge over the target heteroatoms N and S were calculated by application of *MOPAC2009* software [37]. The calculations were carried out on the lowest energy conformation, in vacuum, using the PM3 or PM6 semi-empirical approach and with the eigenvector used as the optimization algorithm.

With respect to the charge distribution pattern in the quinazoline derivatives **3**, highly negative values were obtained – especially for the nitrogens in the pyrimidine ring. The exceptions to this trend are compounds **3g** and **3k**, in which the presence of a halogen (chlorine and bromine, respectively) in the aromatic nucleus at the end of the lateral branches leads to a significant distortion in the pattern, since although N2 and N4 continue to have negative charge values, N1 and N3 in the branch linkage have a partial positive charge.

The pattern for the pyrido[2,3-*d*]pyrimidine derivatives was quite different. All of the 2-(alkylsulfanyl)-*N*-alkylpyrido[2,3-*d*]pyrimidin-4-amine derivatives **6a**–**s** display a parallel distribution in which the negative charges (which are generally less negative than those obtained for compound **3**) are located over the scaffold nitrogens, whereas the heteroatoms pertaining to the linkage present values near to 0 (slightly positive for N1 and slightly negative for S).

With respect to the pyrido[2,3-*d*]pyrimidin-2,4-diamine derivatives, the charge distribution pattern on the target heteroatoms is quite similar to that found for compound **3**, although the presence of N5 (the pyridine ring on the central heteroaromatic nucleus) constitutes a new negative point that could modify the binding mode to the active site. In a similar way to compound **3** (with halogens as substituents), N1 is positive in derivatives **6ab** and **6ae**,

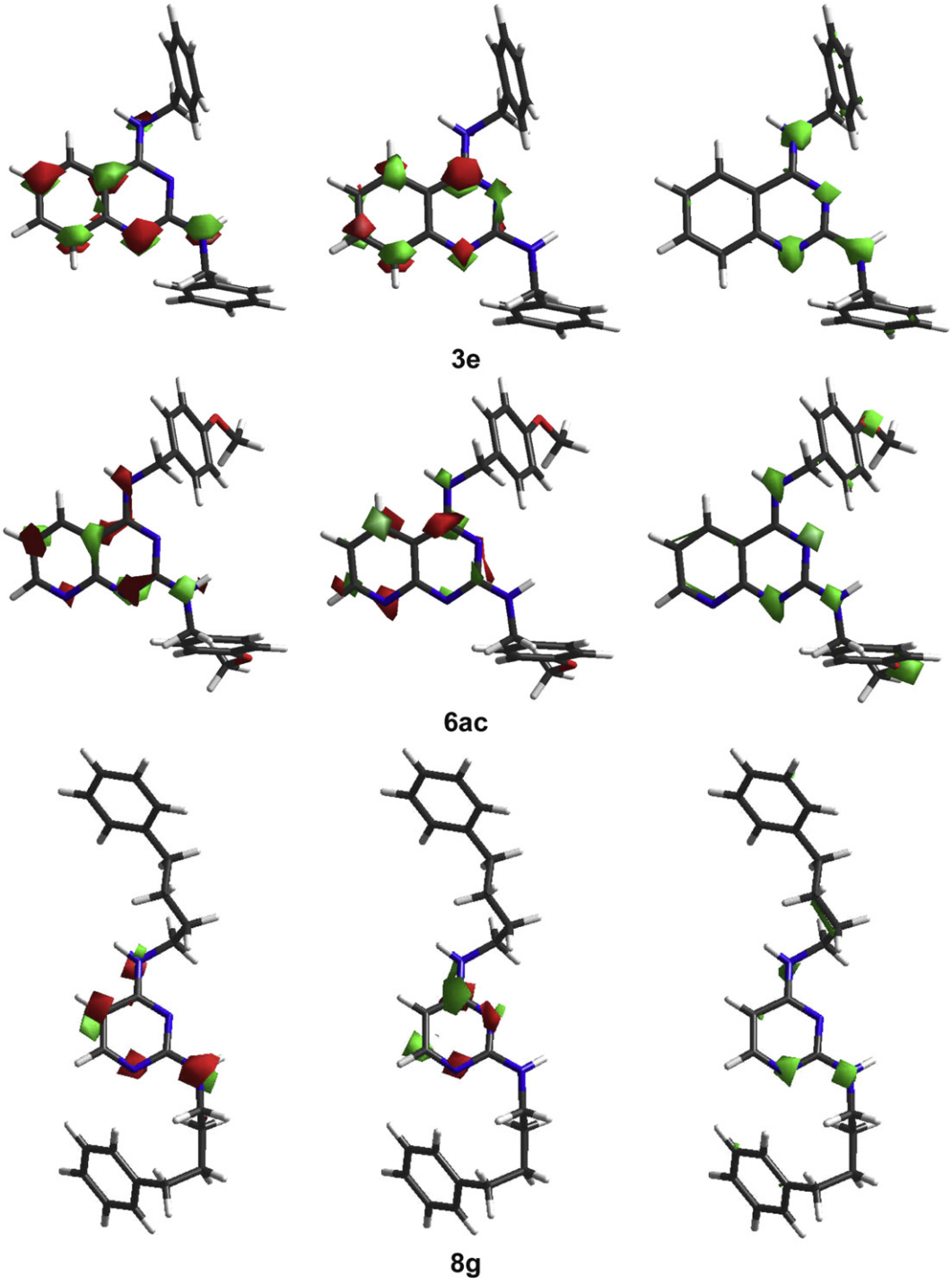

Fig. 6. Schematic HOMO (left), LUMO (middle), MEP (right) distribution for representative active and inactive compounds, calculated from lowest energy conformation.

which contain chlorine and bromine, respectively. The behavior of the heteroatomic charges in derivative **6y** is remarkable in that nitrogens N1 and N4, which are located in linkages, are both positive. As previously noted in the conformational analysis, the preferred conformation for the derivatives bearing a hydroxyl group at the end of the lateral branches is the one in which these side chains are folded towards the central ring; in this way intramolecular hydrogen bonds can be formed that can alter the charge distribution of these derivatives.

The gap is sometimes considered as a measure of the excitability of the molecule: i.e., the lower the energy, the more easily it will be excited. As far as the gap is concerned, it can be observed that compound **8** generally have a higher gap than compounds **3** and **6**. Thus, for the analyzed **8** derivatives the mean gap value is greater than 8.5 eV, whereas for 2-(alkylsulfanyl)-*N*-alkylpyrido[2,3-*d*] pyrimidin-4-amine derivatives the mean gap is near to 7.7 eV. With respect to the pyrido[2,3-*d*]pyrimidin-2,4-diamine derivatives, the mean gap is near to 8.0 eV, which is similar to the values obtained for the quinazoline derivatives.

The disparity in the data does not allow us to draw firm conclusions with respect to this parameter and its possible influence on the target activity, although generally the compounds with

the most interesting biological profiles (**3e**, **6c**, **6e**, **6j**, **6p**, **6z**, **6ac**) have gap values in the range 7.7–8.0 eV.

As far as the distribution of the HOMO and LUMO orbitals is concerned, all of the compounds display a parallel distribution, with a strong contribution to the HOMO 0 orbital from the S located in the 2-position of the pyrido[2,3-*d*]pyrimidine ring in 2-(alkylsulfanyl)-*N*-alkylpyrido[2,3-*d*]pyrimidin-4-amine derivatives **6a**–**s**.

3. Conclusions

The data obtained in this study allowed us to validate the design process carried out for the compounds under investigation. The preliminary structure–activity relationship proposed can be summarized as follows.

With respect to the evaluated scaffold, the preferred central nucleus proved to be the pyrido[2,3-*d*]pyrimidine unit, in which the nitrogens can act as HBAs.

The selected linkage with the lateral branches is the amino group, which in the case with a nitrogen at position 4 can act as an HBA or HBD, whereas the nitrogen at position 2 acts as an HBD.

The preferred length for the lateral branches is three or four methylene groups or one or two methylene groups with an aromatic nucleus at the end, and the best activity profile was shown by derivatives that bear the same chain in positions 2 and 4 of the central ring. The presence of polar groups at the ends of the lateral amino branches leads to loss of activity. Although the tolerance for the lipophilic values was broad, the best activity data were found for compounds with ALogP 98 values between 4.5 and 5.5.

The lowest energy conformation for the majority of compounds was characterized as type D, in which the NH at position 4 points towards the pyridine ring and the NH at position 2 points towards nitrogen 3 of the pyrimidine ring.

As discussed in our previous reports, the structural profile of the selected compounds (see **3e** and **6ac** structures as an example) is quite different from that deduced on considering the related compounds taken as structural references for our design, particularly in terms of the elements that act as hydrogen bond donor (HBDs) or acceptor (HBAs), the alteration of the substitution pattern in the central nucleus, and the lipophilic profile. Thus, taking Piritrexim as an example of a structurally related antitumoral (Fig. 2), it is worth highlighting the presence of free $-NH_2$ groups at the 2- and 4-positions of the pyrimidine, which presumably act as HBDs, while the nitrogens of the pyrido[2,3-*d*]pyrimidine ring can act as HBAs, and the presence of substituents (e.g., 2,5-dimethoxybenzyl for Piritrexim) at the 6-position of the pyridopyrimidine ring. Concerning compounds **3e** and **6ac**, the nitrogens at positions 2 and 4 act as carriers for benzylic groups, whereas the benzene ring of **3e** or the pyridine ring of **6ac** are unsubstituted (Fig. 2).

On the basis of the analyzed structural profiles, different mechanisms of action can be suggested for the quinazolin-2,4-diamine, the 2-(alkylsulfanyl)-*N*-alkylpyrido[2,3-*d*]pyrimidin-4-amine and the pyrido[2,3-*d*]pyrimidin-2,4-diamine derivatives. The precise mechanism of action of some of these derivatives is currently under investigation in our laboratory. Optimization of our pattern from the structure–activity relationship data, as well as the elucidation of the mechanisms of action, could very well lead to the development of novel drug leads in this field.

4. Experimental protocols

4.1. Chemistry

The synthesis of the new compounds was developed according to previously reported methods, which were adapted to the target derivatives (see Supplementary data for details). All compounds were characterized by ^{1}H NMR (Bruker 400 Ultrashield™, Bruker, Rheinstetten, Germany; TMS as the internal standard), FT-IR (Thermo Nicolet FT-IR Nexus spectrophotometer, Thermo Electron Corporation, Waltham, MA, USA; samples as KBr pellets) and EI-MS (Hewlett–Packard MSD 5973 N spectrometer, GC 6890plus/DIP; Agilent Technologies, Inc., Santa Clara, CA, USA) techniques. The spectroscopic data obtained are consistent with the proposed structures.

The melting points were determined with Mettler FP82 + FP80 apparatus (Mettler–Toledo, Greifensee, Switzerland) and are not corrected. Elemental microanalyses were carried out on vacuum-dried samples using an elemental analyzer (LECO, CHN-900 Elemental Analyzer; LECO Corporation, St. Joseph, MI, USA) and were in an acceptable range of ±0.4% for all compounds.

The experimental and spectroscopic data for the synthesized compounds are provided in Supplementary data.

4.1.1. 1,2,3,4-tetrahydro-2,4-dioxopyrido[2,3-d]pyrimidine (**4**)

From 2-aminonicotinic acid and urea, according to previously reported methods [11].

4.1.2. 2,4-dichloropyrido[2,3-d]pyrimidine (**5**)

A mixture **4** (6.0 mmol), $POCl_3$ (5 mL) and *N*,*N*-DMF (catalytic amount) was stirred and heated under reflux for 48 h. The solvents were removed under vacuum and cold water (0 °C, 25 mL) and chloroform (25 mL) were added. The organic layer was washed with water (3 × 20 mL) and dried over anhydrous sodium sulfate. The solvent was removed under vacuum and the product was used immediately without further purification.

4.1.3. General procedure for compound **6**

A mixture of **5** (5.0 mmol), the respective amine (12 mmol), equimolecular amounts of triethylamine, and ethanol (15 mL) was heated at 70 °C for 5 h with stirring. The solvent was removed under vacuum and the residue was dissolved in water (30 mL); the mixture was extracted with chloroform (3 × 25 mL) and the organic extracts were dried over anhydrous sodium sulfate and the solvent was removed in vacuum.

4.1.3.1. N,N′-dihexylaminopyrido[2,3-d]pyrimidin-2,4-diamine (**6v**).

From hexylamine.

4.1.3.2. N,N′-bis(3-hydroxypropyl)pyrido[2,3-d]pyrimidin-2,4-diamine (**6x**).

From 3-amino-1-propanol.

4.1.3.3. N,N′-bis(4-hydroxybutyl)pyrido[2,3-d]pyrimidin-2,4-diamine (**6y**).

From 4-amino-1-butanol.

4.1.4. General procedure for compound **8**

A mixture of commercially available 2,4-dichloropyrimidine **4** (10 mmol), the selected amine (30 mmol), equimolecular amounts of triethylamine and ethanol (15 mL) was heated at 70 °C for 5 h with stirring. The solvent was removed under vacuum and the residue was washed with 5% HCl (25 mL). The resulting solid was isolated and purified by recrystallization.

4.1.4.1. N,N′-dibenzylaminopyrimidin-2,4-diamine (**8a**).

From benzylamine.

4.1.4.2. N,N′-bis(4-methylphenyl)methylpyrimidin-2,4-diamine (**8b**).

From 4-methylbenzylamine.

4.1.4.3. N,N′-bis(4-chlorophenyl)methylpyrimidin-2,4-diamine (**8c**).

From 4-chlorobenzylamine.

*4.1.4.4. N,N′-bis(4-methoxyphenyl)methylpyrimidin-2,4-diamine (**8d**).* From 4-methoxybenzylamine.

*4.1.4.5. N,N′-bis(2-phenylethyl)pyrimidin-2,4-diamine (**8e**).* From 2-phenylethylamine.

*4.1.4.6. N,N′-bis(3-phenylpropyl)pyrimidin-2,4-diamine (**8f**).* From 3-phenylpropylamine.

*4.1.4.7. N,N′-bis(4-phenylbutyl)pyrimidin-2,4-diamine (**8g**).* From 4-phenylbutylamine.

4.2. Biological assays

The five human cell lines were obtained from the American Tissue Culture Collection (Manassas, VA, USA): HT-29 (ATCC HTB 38) is a colon adenocarcinoma cell line, T-24 (ATCC HTB-24) was obtained from urinary bladder cancer, MDA-MB-231 (ATCC HTB26) was established from adenocarcinoma of mammary gland, CRL-8799 was obtained from breast epithelium (ATCC 184B5) and CRL-11233 (ATCC THLE-3) from human liver. HT-29 and T-24 cells were cultured in McCoy's medium (Gibco–Invitrogen, Barcelona, Spain), MDA-MB-231 in Leibovitz (Gibco), CRL-8799 in MEG (Clonetics Corporation) and CRL-11233 in BEGM (BEGM Bullet kit, Clonetics Corporation, San Diego, CA, USA). These media were supplemented with 10% fetal bovine serum, penicillin (50 U/mL) and streptomycin (50 μg/mL). Cells were grown as a monolayer in 175 mL flasks (Corning) and were incubated at 37 °C in a humidified atmosphere containing 5% CO_2. The evaluated compounds were dissolved in dimethylsulfoxide (DMSO). The DMSO concentration was equalized in all media. In all cases, the concentration of solvent in the culture medium did not exceed 0.5% (v/v).

The evaluation of cytotoxic potential and selectivity against human cell lines was determined according to previously reported methods [9,10], by using the neutral red assay as described by Lowik et al. [38] (see Supplementary data for details). Survival percentage was determined at the screening concentrations of 20 and 100 μM, using the survival percentage obtained with the cells treated only with the solvent (DMSO at 0.5%) as a reference.

The results are expressed as the average of triplicate assays. IC_{50} values were calculated for those compounds showing less than 45% survival in the cell lines at 100 μM concentration. This value was determined in triplicate by curvilinear-regression analysis using the statistical program SPSS 11.0 (SPSS Inc., Chicago, IL, USA).

With regard to selectivity, cytotoxicity was determined in cell cultures of two non-tumoral lines, CRL-7899 and CRL-11233. The highest IC_{50} calculated in the three tumoral lines was selected as the test concentration for assays on non-tumoral cells.

The apoptosis induction in human cancer cell lines was quantified through the DNA fragmentation detected at 48 h after treatment using the Cell Death detection ELISA Plus kit (Roche Diagnostics, Indianapolis, IN, USA) according to previously reported methods [9,10]. A relative value of 1 was attributed to the apoptosis detected in the control cultures in which the test compound was not present.

The evaluation of caspase-3 activation was carried out by means of cytometry, using the Active-Caspase-3 FITC Mab apoptosis kit (Pharmingen), according to previously reported methods [9,10]. Measurements were taken at 14, 24 and 48 h and the values obtained were compared with those of control cells incubated without the test compounds. The test concentrations correspond to the IC_{50} values determined in the cytotoxicity assay. Cytometry was performed on a FACSCAN (Becton Dickinson).

4.3. Molecular modeling

The initial computational work was performed on a Dell Precision 380 workstation provided with the software package Discovery Studio 2.5v (DS 2.5v) and with the *MOPAC2009* package.

The starting atomic coordinates were obtained from the structurally related Brookhaven Protein Data Bank (PDB) and CSD structures cited above (CSD System version 5.31: search and information retrieval with ConQuest version 1.12 [39], structure visualization with Mercury CSD [39] version 2.3).

The three-dimensional models of the studied compounds were constructed, in the vacuum phase, using as starting fragments the PDB and CSD related structures, as well as atoms and structural fragments from the Viewer module (DS 2.5v) and using the Dreiding force field [40]. Once the models had been constructed, a preliminary conformational analysis was carried out. The applied protocol (Diverse Conformational Generation integrated DS 2.5v protocol) can be summed up as follows: (a) Initial construction of the model and first minimization by application of the Dreiding minimize protocol (steepest descent algorithm with a convergence criterion of 10^{-6}). The AlogP 98 [24,25] descriptor (an implementation of the atom-based ALogP method) was calculated for each compound. (b) Application of the BEST routine for conformation generation (first: conjugate-gradient minimization in torsion space; second: conjugate-gradient minimization in Cartesian space; third: Quasi–Newton minimization in Cartesian space). (c) Elimination of those conformations whose relative energy is greater than 10 kcal/mol at a global minimum. (d) Analysis of conformational trajectory and selection of representative lowest energy conformations. Root mean square (rms) deviations of the structures were monitored. The energy differences between the different conformations analyzed for each trajectory were around 5 kcal.

For each of the compounds, 25–30 lowest energy conformations were selected and a new minimization cycle was applied. The volumes of the whole molecule were also calculated.

The molecular electrostatic potential (MEP) values were calculated using the DS 2.5v implemented Electrostatic Potential Protocol (EPP). This protocol calculates the electrostatic potential of a molecule by solving a nonlinear Poisson–Boltzmann equation using the finite difference method [41], as implemented in the DS Delphi 4v [42,43] release 1.1 algorithm. The potential was calculated on grid points per side ($65 \times 65 \times 65$) and the percentage of box to be filled was set to 50%. The outer dielectric and the dielectric in the medium were set to 80.0 and 2.0, respectively. An ionic exclusion radius of 2.0 Å, a solvent radius of 1.4 Å, and a solvent ionic strength of 0.145 M were applied. CHARMM [44,45] charges and radii were used for this calculation.

The mechano-quantic analysis of the conformations obtained in the previous step was carried out with the package *Mopac2009*, PM6 [46] (or PM3 [47] for halogen and/or sulfur-containing derivatives) semi-empirical approaches, with the geometry optimized using an eigenvector following algorithm. The energy and distribution of the HOMO and LUMO orbitals, the atomic charges, the electronic density (ED) and the dipolar moment were obtained for each of the conformations. The data corresponding to the mean value of the representative low energy conformations, selected from the conformational trajectory for each compound, was used to establish the preliminary structure–activity relationships.

Acknowledgments

The authors wish to express their gratitude to M.V. Domínguez, J. Ramiro, X. Sáenz, S. Leoz, M. Echeverría, H. Chozas and E. Ardaiz for their collaboration in the synthetic processes and to J. García-

Foncillas, L. Cordeu and E. Cubedo for their collaboration in the biological evaluation.

Appendix. Supplementary material

Supplementary material can be found, in the online version, at doi:10.1016/j.ejmech.2011.05.060.

References

[1] K.M. Hajra, J.R. Liu, Apoptosis 9 (2004) 691–704.
[2] J.C. Reed, Cancer. Cell. 3 (2003) 17–22.
[3] J. Baselga, S.M. Swain, Nat. Rev. Cancer. 9 (2009) 463–465.
[4] C.H.J. Brown, S. Lain, C.H.S. Verma, A.R. Fersht, D.P. Lane, Nat. Rev. Cancer. 9 (2009) 862–873.
[5] C. Sanmartín, M. Echeverría, B. Mendivil, L. Cordeu, E. Cubedo, J. García-Foncillas, M. Font, J.A. Palop, Bioorg. Med. Chem. 13 (2005) 2031–2044.
[6] C. Sanmartín, E. Ardaiz, L. Cordeu, E. Cubedo, J. García-Foncillas, M. Font, J.A. Palop, Lett. Drug Des. Discovery 2 (2005) 341–354.
[7] M. Font, E. Ardaiz, L. Cordeu, E. Cubedo, J. García-Foncillas, C. Sanmartín, J.A. Palop, Bioorg. Med. Chem. 14 (2006) 1942–1948.
[8] E. Echeverría, B. Mendívil, L. Cordeu, E. Cubedo, J. García-Foncillas, M. Font, C. Sanmartín, J.A. Palop, Arch. Pharm. Chem. Life Sci. 339 (2006) 182–192.
[9] E. Cubedo, L. Cordeu, E. Bandrés, A. Rebollo, R. Malumbres, C. Sanmartín, M. Font, J.A. Palop, J. García-Foncillas, Cancer. Biol. Ther. 5 (2006) 850–859.
[10] L. Cordeu, E. Cubedo, E. Bandres, A. Rebollo, X. Saenz, H. Chozas, M.V. Domínguez, M. Echeverría, B. Mendívil, C. Sanmartín, J.A. Palop, M. Font, J. García-Foncillas, Bioorg. Med. Chem. 15 (2007) 1659–1669.
[11] C. Sanmartín, M.V. Domínguez, L. Cordeu, E. Cubedo, J. García-Foncillas, M. Font, J.A. Palop, Arch. Pharm. Chem. Life Sci. 341 (2008) 28–41.
[12] M. Vieth, M. Siegel, Structural fragments in marketed oral drugs Ch. 6. in: W. Jahnke, D.A. Erlanson (Eds.), Fragment Based Drug Discovery. Wiley-VCH Verlag GmbH & Co. KGaA, 2006.
[13] M. Vieth, M.G. Siegel, R.E. Higgs, I.A. Watson, D.H. Robertson, K.A. Savin, G.L. Durst, P.A. Hipskind, J. Med. Chem. 47 (2004) 224–232.
[14] J.J. Sutherland, R.E. Higgs, I. Watson, M. Vieth, J. Med. Chem. 51 (2008) 2689–2700.
[15] C. Sanmartín, M. Font, J.A. Palop, Mini-Rev. Med. Chem. 6 (2006) 639–650.
[16] M.Y. Cha, K.O. Lee, J.W. Kim, C.H.G. Lee, J.Y. Song, Y.H. Kim, G.S. Lee, S.B. Park, M.S. Kim, J. Med. Chem. 52 (2009) 6880–6888.
[17] J.A. Bikker, N. Brooijmans, A. Wissner, T.S. Mansour, J. Med. Chem. 52 (2009) 1493–1509.
[18] J.R. Pollard, M. Mortimore, J. Med. Chem. 52 (2009) 2629–2651.
[19] S. Nandi, M.C. Bagchi, Mol. Divers. 14 (2010) 27–38.
[20] T. Hida, S. Ogawa, J.C. Park, J.Y. Park, J. Shimizu, Y. Horio, K. Yoshida, Expert. Rev. Anticancer. Ther. 9 (2009) 17–35.
[21] C. Schettino, M.A. Bareschino, V. Ricci, F. Ciardiello, Expert Rev. Respir. Med. (2008) 167–168.
[22] M. Zink, H. Lanig, R. Troschütz, Eur. J. Med. Chem. 39 (2004) 1079–1088.
[23] H.J. Park, Y.S. Kim, J.S. Kim, E.J. Lee, Y.J. Yi, H.J. Hwang, M.E. Suh, C.K. Ryu, S.L. Lee, Bioorg. Med. Chem. 14 (2004) 3385–3388.
[24] V.N. Viswanadhan, A.K. Ghose, G.R. Revankar, R.K. Robins, J. Chem. Inf. Comput. Sci. 29 (1989) 163–172.
[25] A.K. Ghose, V.N. Viswanadhan, J.J. Wendolowski, J. Phys. Chem. A. 102 (1998) 3762–3372.
[26] D. Barnum, J. Greene, A. Smellie, P. Sprague, J. Chem. Inf. Comput. Sci. 36 (1996) 563–571.
[27] S. Putta, G.A. Landrum, J.E. Penzotti, J. Med. Chem. 48 (2005) 3313–3318.
[28] F.H. Allen, Acta. Crystallogr. B58 (2002) 380–388.
[29] H.M. Berman, J. Westbrook, Z. Feng, G. Gilliland, T.N. Bhat, H. Weissig, I.N. Shindyalov, P.E. Bourne, Nucleic. Acids. Res. 28 (2000) 235–242.
[30] H.M. Berman, K. Henrick, H. Nakamura, Nat. Struct. Biol. 10 (2003) 980.
[31] R. Tanaka, M. Hamamura, A. Tanaka, N. Hirayama, Anal. Sci. 20 (2004) 173.
[32] P.A. Sutton, V. Cody, J. Am. Chem. Soc. 10 (1988) 6219.
[33] V. Cody, J.R. Luft, W. Pangborn, A. Gangjee, Acta Crystallogr. Sect. D 59 (2003) 1603–1609.
[34] P.A. Sutton, V. Cody, J. Med. Chem. 30 (1987) 1843–1848.
[35] M. Liu, S. Wang, J.E. Clampit, R.J. Gum, D.L. Haasch, C.M. Rondinone, J.M. Trevillyan, C. Abad-Zapatero, E.H. Fry, H.L. Sham, G. Liu, Bioorg. Med. Chem. Lett. 17 (2007) 668–672.
[36] C.A. Lipinski, F. Lombardo, B.W. Dominy, P.J. Feeney, Adv. Drug. Deliv. Rev. 23 (1997) 3–25.
[37] MOPAC2009, J.P. Stewart, Stewart Computational Chemistry, version 9.062L web, <http://OpenMOPAC.net>.
[38] C.W. Lowik, M.J. Alblas, M. van de Ruit, S.E. Papapoulos, G. van der Pluijm, Anal. Biochem. 213 (1993) 426–433.
[39] I.J. Bruno, J.C. Cole, P.R. Edgington, M. Kessler, C.F. Macrae, P. McCabe, J. Pearson, R. Taylor, Acta. Crystallogr. B58 (2002) 389–397.
[40] S.L. Mayo, B.D. Olafson, W.A. Goddard, J. Phys. Chem. 94 (1990) 8897–8909.
[41] W. Rocchia, S. Sridharan, A. Nicholls, E. Alexov, A. Chiabrera, B. Honig, J. Comput. Chem. 23 (2002) 128–137.
[42] M.K. Gilson, B. Honig, Protein Struct. Funct. Genet. 4 (1988) 7–18.
[43] W. Rocchia, E. Alexov, B. Honig, J. Phys. Chem. B. 105 (2001) 6507–6514.
[44] B.R. Brooks, R.E. Bruccoleri, B.D. Olafson, D.J. States, S. Swaminathan, M. Karplus, J. Comput. Chem. 4 (1983) 187–217.
[45] A.D. MacKerell, B. Brooks, C.L. Brooks, L. Nilsson, B. Roux, Y. Won, M. Karplus, in: P.v.R. Schleyer (Ed.), The Encyclopedia of Computational Chemistry, Wiley, Chichester, U.K, 1998, pp. 271–277.
[46] J.J.P. Stewart, J. Mol. Model. 13 (2007) 1173–1213.
[47] J.J.P. Stewart, J. Comput. Chem. 10 (1989) 209–220.